Naval Research Laboratory
Washington, DC 20375-5320

Ballistics Modeling for Non-Axisymmetric Hypervelocity Smart Bullets

D.F. Gordon
B. Hafizi

Beam Physics Branch
Plasma Physics Division

Y.-Y. Khine

DoD PETTT
Dynamics Research Corporation
Andover, Massachusetts

S. Douglass

Charged Particle Physics Branch
Plasma Physics Division

June 3, 2014

REPORT DOCUMENTATION PAGE

Form Approved
OMB No. 0704-0188

1. REPORT DATE *(DD-MM-YYYY)*	2. REPORT TYPE	3. DATES COVERED *(From - To)*
03-06-2014	Interim	October 2013 – February 2014

4. TITLE AND SUBTITLE

Ballistics Modeling for Non-Axisymmetric Hypervelocity Smart Bullets

5a. CONTRACT NUMBER

5b. GRANT NUMBER

5c. PROGRAM ELEMENT NUMBER

6. AUTHOR(S)

D.F. Gordon, B. Hafizi, Y.-Y. Khine,[1] and S. Douglass

5d. PROJECT NUMBER
67-6754-04

5e. TASK NUMBER

5f. WORK UNIT NUMBER

7. PERFORMING ORGANIZATION NAME(S) AND ADDRESS(ES)

Naval Research Laboratory
4555 Overlook Avenue, SW
Washington, DC 20375-5320

8. PERFORMING ORGANIZATION REPORT NUMBER

NRL/MR/6790--14-9549

9. SPONSORING / MONITORING AGENCY NAME(S) AND ADDRESS(ES)

Office of Naval Research
875 North Randolph Street, Suite 1425
Arlington, VA 22203-1995

10. SPONSOR / MONITOR'S ACRONYM(S)

ONR

11. SPONSOR / MONITOR'S REPORT NUMBER(S)

12. DISTRIBUTION / AVAILABILITY STATEMENT

Approved for public release; distribution is unlimited.

13. SUPPLEMENTARY NOTES

[1]DoD PETTT, Dynamics Research Corporation, Andover, MA; on-site at NRL.

14. ABSTRACT

A method for calculating the trajectories of guided, non-axisymmetric, hypervelocity projectiles is developed. The method is based on the equations of motion for a rigid body with an internal skid weight and roll wheel, combined with a tabulated set of ballistic coefficients used to specify the aerodynamic forces and moments on the body. The ballistic coefficients can in principle come from experiments or computational fluid dynamics (CFD) calculations. CFD calculations are carried out for a standard bullet (0.308" 168 grain Sierra International) in order to characterize the accuracy given various mesh sizes. The ballistics model is applied to a standard rifle shot in order to demonstrate the epicyclic pitch and yaw behavior. It is then applied to a smart bullet that utilizes a preliminary autopilot algorithm.

15. SUBJECT TERMS

Ballistics
Hypervelocity

Railgun

16. SECURITY CLASSIFICATION OF:			17. LIMITATION OF ABSTRACT	18. NUMBER OF PAGES	19a. NAME OF RESPONSIBLE PERSON
a. REPORT	**b. ABSTRACT**	**c. THIS PAGE**	Unclassified Unlimited	27	Daniel Gordon
Unclassified Unlimited	Unclassified Unlimited	Unclassified Unlimited			**19b. TELEPHONE NUMBER** *(include area code)* (202) 767-5036

Standard Form 298 (Rev. 8-98)
Prescribed by ANSI Std. Z39.18

Ballistics Modeling for non-Axisymmetric Hypervelocity Smart Bullets

D.F. Gordon and B. Hafizi

Beam Physics Branch, Plasma Physics Division

Y.-Y. Khine

Dynamics Research Corporation, HPC PETTT On-Site

S. Douglass

Charged Particle Physics Branch, Plasma Physics Division

A method for calculating the trajectories of guided, non-axisymmetric, hypervelocity projectiles is developed. The method is based on the equations of motion for a rigid body with an internal skid weight and roll wheel, combined with a tabulated set of ballistic coefficients used to specify the aerodynamic forces and moments on the body. The ballistic coefficients can in principle come from experiments or computational fluid dynamics (CFD) calculations. CFD calculations are carried out for a standard bullet (0.308" 168 grain Sierra International) in order to characterize the accuracy given various mesh sizes. The ballistics model is applied to a standard rifle shot in order to demonstrate the epicyclic pitch and yaw behavior. It is then applied to a smart bullet that utilizes a preliminary autopilot algorithm.

Contents

I. INTRODUCTION

This report is concerned with calculating the trajectory of the projectile fired from an electromagnetic launcher, or railgun, which attains supersonic velocity (up to 1500 m/s). Emphasis is given to the projectile which may carry with it the structure that sustains the electrical currents that drive the acceleration in the barrel. This structure, or "armature," does not possess axisymmetry, and its aerodynamic properties are therefore expected to be somewhat novel. An important question is whether such a projectile can be accurately guided toward a target. To address this question theoretically, an advanced exterior ballistics model is needed. The model must not assume axisymmetry, be able to handle hypersonic velocities, and incorporate some form of autopilot algorithm.

Generally, a bullet cannot be designed solely based on aerodynamic considerations. Ordinary bullets, before they are even fired, have to take a form compatible with the requirements of a robust casing. During firing, they have to form a temporary high pressure seal, such that expanding gases can only escape by pushing the bullet out of the barrel. While in the barrel, they have to make suitable contact with the rifling, in order to acquire spin. If it were not for these considerations, one might use a shape such as the Sears-Haack form, which gives the minimum drag at supersonic speeds [1]. In the case of a railgun, there is no requirement involving a casing or high pressure seal. Instead, there is a requirement involving the armature. The armature has roughly a "U" shape, with the two upright segments of the U forming a sliding contact with the rails. The direction of motion is from the top to the bottom of the U. One can either let the armature fall away from whatever projectile it forces out of the barrel, or keep the armature as part of the projectile. The latter scenario is energetically more efficient, but requires that the armature satisfy whatever aerodynamic requirements follow from the mission being considered.

The solution of an exterior ballistics problem gives the position and orientation of a rigid body as a function of time, given a certain set of initial conditions. This involves solving the equations of motion for a rigid body in the presence of aerodynamic forces and moments. Determining the aerodynamic forces and moments under a given set of conditions is extremely complex. Ideally, both numerical solutions of the Navier-Stokes equations, and experimental measurements, are employed. This report discusses how to systematically enumerate the aerodynamic forces and moments, how to quantify them based on available

data, and how to calculate the resultant trajectories.

II.   GENERALIZED BALLISTICS MODEL

A.   Coordinate Systems and Reference Frames

The equations of motion describing the flight of a projectile take their simplest form in an inertial frame of reference. A coordinate system fixed with respect to the ground is not inertial, primarily due to the Earth's rotation. One can still choose to work in such a frame, but then new forces, such as the Coriolis force, appear in the equations of motion. An alternative, which will be employed here, is to work in a frame that has the Earth's rotation subtracted out. Such a frame is inertial to a good enough approximation for most purposes. The coordinates used to describe the components of a vector are distinct from the frame of reference in which the dynamical equations are expressed. In particular, the coordinate basis can be changed without changing the form of the equations. There are four bases that are frequently used in this report. All four bases are illustrated in Fig. 1, which is explained in detail as follows.

The inertial basis is characterized by basis vectors $(\mathbf{i}_1, \mathbf{i}_2, \mathbf{i}_3)$, which are defined so that initially, they line up with the Earth system basis vectors $(\mathbf{e}_1, \mathbf{e}_2, \mathbf{e}_3)$. In turn, the Earth basis is defined so that $\mathbf{e}_1$ points down-range horizontally, and $\mathbf{e}_2$ points up. The equations relating the basis vectors, the initial projectile velocity, $\mathbf{v}_0$, and the initial gravitational acceleration, $\mathbf{g}_0$, are

$$\mathbf{i}_1 = \mathbf{e}_1(t=0) = \frac{\mathbf{g}_0' \times (\mathbf{v}_0' \times \mathbf{g}_0')}{|\mathbf{g}_0' \times (\mathbf{v}_0' \times \mathbf{g}_0')|} \tag{1a}$$

$$\mathbf{i}_2 = \mathbf{e}_2(t=0) = -\frac{\mathbf{g}_0'}{|\mathbf{g}_0'|} \tag{1b}$$

$$\mathbf{i}_3 = \mathbf{e}_3(t=0) = \mathbf{i}_1 \times \mathbf{i}_2 \tag{1c}$$

where the prime is to stress that the velocity and gravitational acceleration are given in the Earth frame of reference. They can be put in the inertial frame using

$$\mathbf{v}_0 = \mathbf{v}_0' + \mathbf{\Omega}_E \times \mathbf{R}_E \tag{2a}$$

$$\mathbf{g}_0 = \mathbf{g}_0' + \mathbf{\Omega}_E \times (\mathbf{\Omega}_E \times \mathbf{R}_E) \tag{2b}$$

where $\mathbf{R}_E$ is a vector drawn from the center of the Earth to the launch site, and $\mathbf{\Omega}_E$ is the
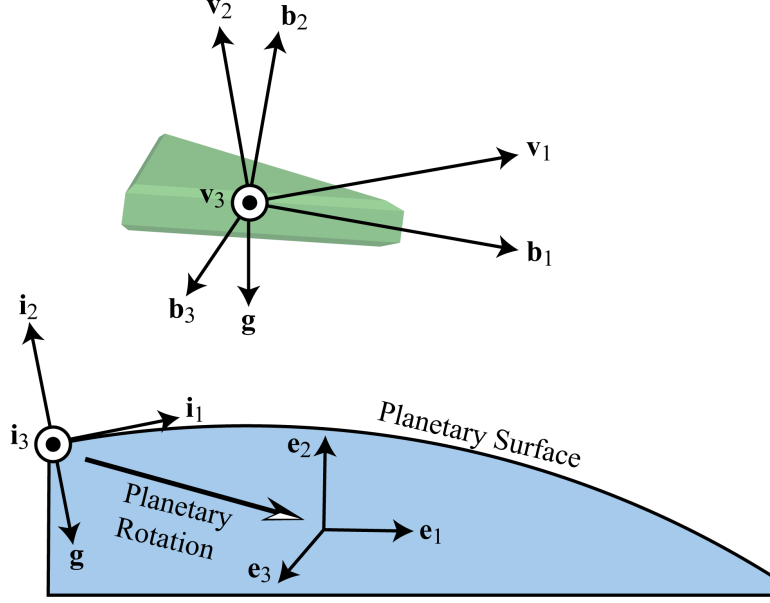
FIG. 1: Schematic of the four sets of basis vectors used to describe the projectile flight. The inertial basis $(\mathbf{i}_1, \mathbf{i}_2, \mathbf{i}_3)$ is fixed by the projectile velocity and gravity at the moment of launch. The Earth basis $(\mathbf{e}_1, \mathbf{e}_2, \mathbf{e}_3)$ is initially the same as $(\mathbf{i}_1, \mathbf{i}_2, \mathbf{i}_3)$ but rotates with the planetary surface. The velocity basis $(\mathbf{v}_1, \mathbf{v}_2, \mathbf{v}_3)$ is fixed by the projectile velocity, wind velocity, and gravity. The body basis $(\mathbf{b}_1, \mathbf{b}_2, \mathbf{b}_3)$ is fixed with respect to the symmetry planes of the projectile.

angular velocity of the Earth. As the Earth rotates, $(\mathbf{e}_1, \mathbf{e}_2, \mathbf{e}_3)$ evolve according to

$$\frac{d\mathbf{e}_i}{dt} = \mathbf{\Omega}_E \times \mathbf{e}_i \tag{3}$$

where i is any of the coordinate indices. Similarly, the launch site moves in the inertial frame according to

$$\frac{d\mathbf{R}_E}{dt} = \mathbf{\Omega}_E \times \mathbf{R}_E \tag{4}$$

Distinguishing the Earth system from the inertial system allows one to consider range scales that are an arbitrary fraction of the radius of the Earth.

A system of coordinates that rotates with the body is not very useful as a reference frame, but is indispensible as a coordinate basis. The body basis, $(\mathbf{b}_1, \mathbf{b}_2, \mathbf{b}_3)$, is defined so that $\mathbf{b}_1$ always points in the direction of the nose. For a railgun projectile, $\mathbf{b}_2$ is in the plane of the rail surfaces, and $\mathbf{b}_3$ is orthogonal to it. The time evolution of $(\mathbf{b}_1, \mathbf{b}_2, \mathbf{b}_3)$ during the projectile flight is a primary concern of the ballistics problem, as discussed below.

Finally, the velocity basis, $(\mathbf{v}_1, \mathbf{v}_2, \mathbf{v}_3)$, changes with the projectile velocity, the wind, and
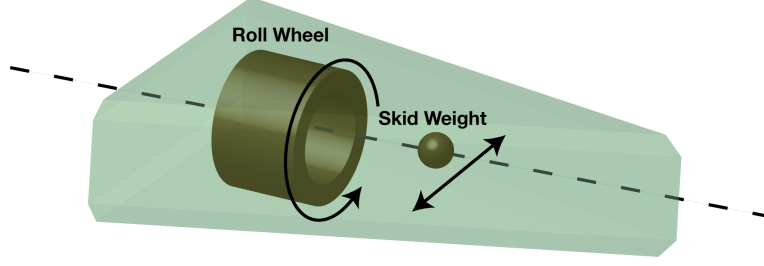
FIG. 2: Abstract representation of projectile. The moving parts consist of a roll wheel and skid weight. The roll wheel rotates about the longitudinal axis, but is otherwise fixed in the body. The skid weight is a movable point mass which is unconstrained for the purposes of analysis.

the gravitational acceleration. If the projectile velocity is $\mathbf{v}$, and the wind velocity is $\mathbf{w}$, then

$$\mathbf{v}_1 = \frac{\mathbf{v} - \mathbf{w}}{|\mathbf{v} - \mathbf{w}|} \tag{5a}$$

$$\mathbf{v}_2 = \mathbf{v}_3 \times \mathbf{v}_1 \tag{5b}$$

$$\mathbf{v}_3 = \frac{\mathbf{g} \times (\mathbf{v} - \mathbf{w})}{|\mathbf{g} \times (\mathbf{v} - \mathbf{w})|} \tag{5c}$$

Note that if the net velocity is directly up or down, then $\mathbf{v}_2$ and $\mathbf{v}_3$ are undefined. As will be seen below, this turns out to be unimportant, as only $\mathbf{v}_1$ is used in the dynamical equations.

B.   The Modified Rigid Body Problem

In order for a projectile to have a steering capability, it cannot be entirely rigid. In this report, steering by means of internal moving parts is considered. The total system is a rigid body plus an unconstrained point mass, or "skid weight," and a rotatable ring, or "roll wheel." When the skid weight is moved, the center of mass moves, inducing a pitching moment. When the roll wheel is rotated, a rolling moment is induced. Of course, an energy source is needed to move these parts. The skid weight is efficient, since it turns the projectile indirectly, through its effect on aerodynamic forces. The roll wheel, in contrast, is actually opposed by aerodynamic forces, and so may not be very practical. In this report, the energy source that moves the internal parts is not considered.

Let $\mathbf{r}_0$ be the center of mass of the whole projectile, and let the skid weight position be $\mathbf{d}$. We define $\mathbf{R}$ as where the center of mass would be if the skid weight were absent. It is convenient to use $\mathbf{R}$ as the reference point, because it is fixed with respect to the rigid

portion of the body. If the mass of the skid weight is δm, then the displacement of the center of mass is

$$\mathbf{a} \equiv \mathbf{r}_0 - \mathbf{R} = \frac{\delta m}{m}(\mathbf{d} - \mathbf{R}) \tag{6}$$

where m is the mass of the whole projectile. The translational motion is described by

$$\mathbf{P} = m\mathbf{v} + \delta m \delta \mathbf{v} + m\boldsymbol{\Omega} \times \mathbf{a} \tag{7a}$$

$$\dot{\mathbf{P}} = \mathbf{F} + m\mathbf{g} \tag{7b}$$

$$\dot{\mathbf{R}} = \mathbf{v} \tag{7c}$$

where $\mathbf{P}$ is the total momentum, $\mathbf{v}$ is the velocity of the reference point, $\mathbf{F}$ is the sum of all aerodynamic forces, $\mathbf{g}$ is the gravitational acceleration, $\boldsymbol{\Omega}$ is the angular velocity, and

$$\delta \mathbf{v} = \dot{\mathbf{d}} - \mathbf{v} - \frac{m}{\delta m}\boldsymbol{\Omega} \times \mathbf{a} \tag{8}$$

is the velocity of the skid weight in the body system of reference [6]. Let the roll wheel be centered transversely inside the projectile, with inertia tensor $\delta \mathsf{M}$ and angular velocity $\boldsymbol{\Omega} + \delta\boldsymbol{\Omega}$. Then, the rotational motion is described by

$$\mathbf{L} = \mathsf{M}\boldsymbol{\Omega} + \delta\mathsf{M}\delta\boldsymbol{\Omega} + \mathbf{a} \times (\mathbf{P} + m\delta\mathbf{v}) \tag{9a}$$

$$\dot{\mathbf{L}} = \mathbf{K} \tag{9b}$$

$$\dot{\mathbf{b}}_i = \boldsymbol{\Omega} \times \mathbf{b}_i \tag{9c}$$

where $\mathbf{L}$ is the total angular momentum, $\mathbf{K}$ is the sum of all aerodynamic moments (the torque), and M is the effective inertia tensor of the system. If the inertia tensor of the rigid body is M_0, then the effective inertia tensor is

$$\mathsf{M} = \mathsf{M}_0 + \delta\mathsf{M} + (m - \delta m)\begin{pmatrix} \delta y^2 + \delta z^2 & -\delta x \delta y & -\delta x \delta z \\ -\delta x \delta y & \delta x^2 + \delta z^2 & -\delta y \delta z \\ -\delta x \delta z & -\delta y \delta z & \delta x^2 + \delta y^2 \end{pmatrix} \tag{10}$$

Here, $(\delta x, \delta y, \delta z)$ are the components of $\mathbf{a}$. It is often convenient to express M_0, $\delta\mathsf{M}$, and $\mathbf{a}$ in the $(\mathbf{b}_1, \mathbf{b}_2, \mathbf{b}_3)$ basis. Naturally, all vectors should be expressed in a consistent basis before updating the dynamical equations. In particular, the dynamical equations are most naturally evaluated in the $(\mathbf{i}_1, \mathbf{i}_2, \mathbf{i}_3)$ basis.

Solution of the above system of equations by numerical means presents little difficulty, provided $\mathbf{F}$ and $\mathbf{K}$ are known. The primary problem in solving for the projectile motion is to

determine suitable approximations for **F** and **K** as functions of the body momentum, angular momentum, position, and orientation. This is the purpose of the ballistic coefficients.

III. GENERALIZED BALLISTIC COEFFICIENTS

Ballistic coefficients are usually given for axisymmetric projectiles. The purpose of this section is to derive extended coefficients that treat the more general case of a two-fold inversion symmetry. The approach is to utilize symmetry relations in conjunction with a small angle expansion to deduce the dependence on the body orientation. The dependence on angular momentum is treated using an expansion in angular velocity. Except for Magnus moments, the orientational and angular momentum dependence is assumed additively separable. The dependence on position enters as a dependence on the local atmospheric conditions. The dependence on momentum enters as an overall factor proportional to the kinetic energy density of the fluid, and as a dependence on Mach number that has to be tabulated term by term.

A. Terms due to Body Orientation

1. Orientational Expansion

The most general way to write the dependence of a force on an orientation is in terms of a tensor expansion, i.e.,

$$F^i = a^i + b^i_{jk}T^{jk} + c^i_{jklm}T^{jk}T^{lm} + d^i_{jklmno}T^{jk}T^{lm}T^{no} + \cdots \tag{11}$$

where a, b, c, and d are tensor coefficients that depend on position and Mach number, and T is a tensor expressing the body orientation[7]. One needs a similar equation for **K**. The orientation T^{ij} is expressed in terms of the body and velocity basis vectors according to

$$\mathsf{T} = \begin{pmatrix} \mathbf{b}_1 \cdot \mathbf{v}_1 & \mathbf{b}_2 \cdot \mathbf{v}_1 & \mathbf{b}_3 \cdot \mathbf{v}_1 \\ \mathbf{b}_1 \cdot \mathbf{v}_2 & \mathbf{b}_2 \cdot \mathbf{v}_2 & \mathbf{b}_3 \cdot \mathbf{v}_2 \\ \mathbf{b}_1 \cdot \mathbf{v}_3 & \mathbf{b}_2 \cdot \mathbf{v}_3 & \mathbf{b}_3 \cdot \mathbf{v}_3 \end{pmatrix} \tag{12}$$

Note that this is also the matrix of transformation taking a vector expressed in the body basis into the same vector expressed in the velocity basis.
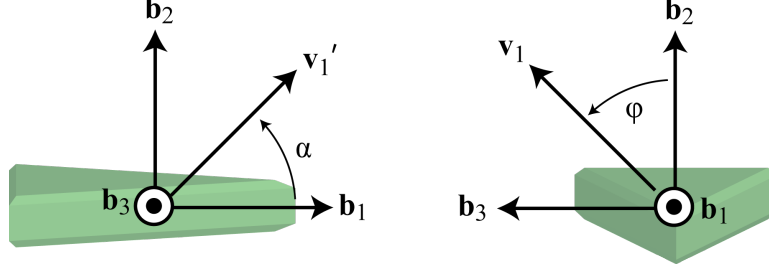
FIG. 3: Expressing the unit vector $\mathbf{v}_1$ in terms of the angles α and φ. The direction of $\mathbf{v}_1$ can be constructed by starting parallel to $\mathbf{b}_1$, rotating through an angle α in the 12-plane to form $\mathbf{v}_1'$, and then through an angle φ in the 23-plane to form $\mathbf{v}_1$. The angles are chosen so $\mathbf{v}_1$ is consistent with Eq. (5).

The expansion (11) involves a great many terms. It is useful to reduce the complexity by reducing the rank of the tensors involved. The major assumption we make is that only the first row of T contains information needed to deduce the forces and moments. The physical justification for this is that $\mathbf{v}_2$ and $\mathbf{v}_3$ are fixed only by gravity, and gravity affects the *aerodynamic* forces and moments very weakly (which is not to say the force of gravity itself is immaterial). The first row of T is $\mathbf{v}_1$ expressed in the body basis, which is itself a tensor of rank one, i.e., a vector. Let the components of $\mathbf{v}_1$ in the body basis be denoted ξ^i. Furthermore, define angles α and φ such that

$$\begin{pmatrix} \xi^1 \\ \xi^2 \\ \xi^3 \end{pmatrix} = \begin{pmatrix} \cos\alpha \\ \sin\alpha\cos\varphi \\ \sin\alpha\sin\varphi \end{pmatrix} \tag{13}$$

This expresses $\mathbf{v}_1$ in spherical coordinates that are referenced to $(\mathbf{b}_1, \mathbf{b}_2, \mathbf{b}_3)$, as illustrated in Fig. 3. The angle α is also what is usually called the total yaw angle, which during gentle maneuvers is small. Hence, the formal expansion

$$F^i = a^i + b^i_j \xi^j + c^i_{jk} \xi^j \xi^k + d^i_{jkl} \xi^j \xi^k \xi^l + \cdots \tag{14}$$

can be ordered in the small parameter α. Note that the components of the force are given in the same basis that the ξ^i are given in, namely the body basis. In this case, one has an axial force, F^1, in place of the drag force, and normal forces F^2 and F^3, in place of the lift force. The relationship between velocity basis coefficients, such as the drag coefficient, with body basis coefficients, is given in the appendix.

2. Symmetry Relations

The ballistics coefficients are further reduced by exploiting symmetry. For a railgun projectile with an integrated armature, axisymmetry is lost, but inversion symmetry holds in the $\mathbf{b}_2$ and $\mathbf{b}_3$ directions. This implies that when the sign of ξ^2 or ξ^3 is changed, the components of the forces and moments, in the body basis, either do not change, or merely change sign, depending on the component considered. For the forces,

$$F^1(\xi^1, \xi^2, \xi^3) = F^1(\xi^1, -\xi^2, \xi^3) \tag{15a}$$

$$F^1(\xi^1, \xi^2, \xi^3) = F^1(\xi^1, \xi^2, -\xi^3) \tag{15b}$$

$$F^2(\xi^1, \xi^2, \xi^3) = -F^2(\xi^1, -\xi^2, \xi^3) \tag{15c}$$

$$F^2(\xi^1, \xi^2, \xi^3) = F^2(\xi^1, \xi^2, -\xi^3) \tag{15d}$$

$$F^3(\xi^1, \xi^2, \xi^3) = -F^3(\xi^1, \xi^2, -\xi^3) \tag{15e}$$

$$F^3(\xi^1, \xi^2, \xi^3) = F^3(\xi^1, -\xi^2, \xi^3) \tag{15f}$$

For the moments,

$$K^1(\xi^1, \xi^2, \xi^3) = -K^1(\xi^1, -\xi^2, \xi^3) \tag{16a}$$

$$K^1(\xi^1, \xi^2, \xi^3) = -K^1(\xi^1, \xi^2, -\xi^3) \tag{16b}$$

$$K^2(\xi^1, \xi^2, \xi^3) = K^2(\xi^1, -\xi^2, \xi^3) \tag{16c}$$

$$K^2(\xi^1, \xi^2, \xi^3) = -K^2(\xi^1, \xi^2, -\xi^3) \tag{16d}$$

$$K^3(\xi^1, \xi^2, \xi^3) = K^3(\xi^1, \xi^2, -\xi^3) \tag{16e}$$

$$K^3(\xi^1, \xi^2, \xi^3) = -K^3(\xi^1, -\xi^2, \xi^3) \tag{16f}$$

These relations can be used to eliminate either odd or even terms in the tensor expansion, greatly reducing the number of terms that have to be considered. The number of independent terms is also greatly reduced simply due to the fact that multiplication commutes, i.e., coefficients that differ by only a permutation of the lower indices can be taken as equal.

3. Orientational Forces

The orientational forces correspond to lift and drag, which in the body basis are resolved into axial and normal forces. Applying the symmetry relations and keeping terms up to

third order in ξ^i gives

$$F^1 = a^1 + b^1_1\xi^1 + c^1_{11}(\xi^1)^2 + c^1_{22}(\xi^2)^2 + c^1_{33}(\xi^3)^2 + \tag{17a}$$

$$d^1_{111}(\xi^1)^3 + 3d^1_{122}\xi^1(\xi^2)^2 + 3d^1_{133}\xi^1(\xi^3)^2 \tag{17b}$$

$$F^2 = \left[b^2_2 + 2c^2_{12}\xi^1 + 3d^2_{112}(\xi^1)^2 + 3d^2_{332}(\xi^3)^2 + d^2_{222}(\xi^2)^2\right]\xi^2 \tag{17c}$$

$$F^3 = \left[b^3_3 + 2c^3_{13}\xi^1 + 3d^3_{113}(\xi^1)^2 + 3d^3_{223}(\xi^2)^2 + d^3_{333}(\xi^3)^3\right]\xi^3 \tag{17d}$$

Expanding to third order in α and gathering like terms gives

$$\frac{F^1}{F^0} = C_{X\alpha^0} + \alpha^2(C_{X\alpha^2c}\cos^2\varphi + C_{X\alpha^2s}\sin^2\varphi) \tag{18a}$$

$$\frac{F^2}{F^0} = \alpha\cos\varphi\left[C^2_{N\alpha^0} + \alpha^2(C^2_{N\alpha^2c}\cos^2\varphi + C^2_{N\alpha^2s}\sin^2\varphi)\right] \tag{18b}$$

$$\frac{F^3}{F^0} = \alpha\sin\varphi\left[C^3_{N\alpha^0} + \alpha^2(C^3_{N\alpha^2c}\cos^2\varphi + C^3_{N\alpha^2s}\sin^2\varphi)\right] \tag{18c}$$

Here, C are the dimensionless orientational force coefficients, subscripted by X for the axial force, and N for the normal force. The subscript α^n refers to the order of α the coefficient multiplies, the subscript c or s refers to multiplication by $\cos^2\varphi$ or $\sin^2\varphi$, and the superscript indicates the component of force affected. The C coefficients are supposed to depend only on Mach number. The characteristic force F^0 is

$$F^0 = \frac{1}{2}\rho(\mathbf{r})V^2A \tag{19}$$

where $\rho(\mathbf{r})$ is the local mass density of the atmosphere, V is the effective velocity $|\mathbf{v} - \mathbf{w}|$, and A is a reference area, typically the largest transverse cross section of the projectile.

4. Orientational Moments

In the general case of two-fold inversion symmetry, an axial moment appears that, of course, vanishes in the axisymmetric case. This moment causes φ to tend toward an integer multiple of $\pi/2$. Since this has an effect reminiscent of "righting a ship," we call it the roll righting moment. The moments are expanded in the components of $\mathbf{v}_1$ just like the forces:

$$K^i = a^i + b^i_j\xi^j + c^i_{jk}\xi^j\xi^k + d^i_{jkl}\xi^j\xi^k\xi^l + \cdots \tag{20}$$

Here, the coefficients a, b, etc., are re-used to avoid notational clutter. Applying the symmetry relations and keeping terms up to third order in ξ^i gives

$$K^1 = 2c^1_{23}\xi^2\xi^3 + 6d^1_{123}\xi^1\xi^2\xi^3 \tag{21a}$$

$$K^2 = \left[b^2_3 + 2c^2_{13}\xi^1 + 3d^2_{113}(\xi^1)^2 + 3d^2_{223}(\xi^2)^2 + d^2_{333}(\xi^3)^2\right]\xi^3 \tag{21b}$$

$$K^3 = \left[b^3_2 + 2c^3_{12}\xi^1 + 3d^3_{112}(\xi^1)^2 + 3d^3_{332}(\xi^3)^2 + d^3_{222}(\xi^2)^2\right]\xi^2 \tag{21c}$$

Expanding to third order in α and gathering like terms gives

$$\frac{K^1}{K^0} = C^1_{M\alpha^2}\alpha^2\sin 2\varphi \tag{22a}$$

$$\frac{K^2}{K^0} = \alpha\sin\varphi\left[C^2_{M\alpha^0} + \alpha^2(C^2_{M\alpha^2c}\cos^2\varphi + C^2_{M\alpha^2s}\sin^2\varphi)\right] \tag{22b}$$

$$\frac{K^3}{K^0} = \alpha\cos\varphi\left[C^3_{M\alpha^0} + \alpha^2(C^3_{M\alpha^2c}\cos^2\varphi + C^3_{M\alpha^2s}\sin^2\varphi)\right] \tag{22c}$$

Here, C are the dimensionless orientational moment coefficients, annotated similarly to the force coefficients. The axial coefficient characterizes the roll righting moment, while the transverse coefficients correspond to the usual overturning moment. The characteristic moment K^0 is given by

$$K^0 = \frac{1}{2}\rho(\mathbf{r})V^2A\ell \tag{23}$$

where ℓ is a length characteristic of the projectile (in the axisymmetric case, the diameter is usually used).

5. Ballistician's Quasi-Expansion

The small angle expansion used above allows one to develop a consistent ordering in the single parameter α. However, experience has evidently shown [2] that if the substitution $\alpha \to \sin\alpha$ is made everywhere in the expressions for the ballistic coefficients, accuracy is improved. In utilizing the quasi-expansion, an important difference between the velocity basis and the body basis should be noted. In the velocity basis, the force is resolved into lift and drag, while in the body basis it is resolved into normal and axial forces. Among these four components of force, only drag has the characteristic of remaining non-zero for any α. In contrast, the axial force vanishes for $\alpha = \pi/2$. In the quasi-expansion, one would like to recover this characteristic of the axial force. This can be easily accomplished by multiplying the axial force by $\cos\alpha$.

B. Terms due to Angular Momentum

1. Slow Spin Expansion

Typically, the dependence of the forces and moments on the angular momentum of the body is weak compared to its dependence on orientation and momentum. A suitable parameter in which to expand this weak dependence is

$$\omega^i = \frac{\ell \Omega^i}{V} \tag{24}$$

In words, this is the ratio of the tangential velocity of a typical body element as it rotates about the reference point, $\mathbf{R}$, to the velocity of the whole body in the atmosphere. The slow spin expansion is then

$$K^i = b^i_j \omega^j + c^i_{jk} \omega^j \omega^k + \cdots \tag{25}$$

where the symbols b and c are re-used. N.b. the above K^i is to be added to the orientational K^i described in section III A. For this reason, including a zero order term would be redundant.

2. Spin and Pitch Damping

In exterior ballistics, the damping of angular momentum is typically separated into "spin damping" and "pitch damping" terms. This terminology conforms well to a rifle bullet, where the angular velocity is strongly peaked in the $\mathbf{b}_1$ direction. In the more general case, spin damping appears on an equal footing in all three coordinates:

$$\frac{K^1}{K^0} = C^1_{Mq} \omega^1 \tag{26a}$$

$$\frac{K^2}{K^0} = C^2_{Mq} \omega^2 \tag{26b}$$

$$\frac{K^3}{K^0} = C^3_{Mq} \omega^3 \tag{26c}$$

Here, a linear approximation is used, with symmetry forbidding linear cross-couplings. The C^1_{Mq} coefficient is what ballisticians call the spin damping coefficient, conventionally denoted C_{lp}. After assuming axisymmetry, C^2_{Mq} and C^3_{Mq} would be combined into a single C_{Mq} called the pitch damping coefficient.

3. Magnus Moment

The Magnus force is seldom important in exterior ballistics, even for a rapidly spinning rifle bullet [2]. However, the Magnus *moment* can be important in terms of stability. The Magnus moment is the one effect we consider where the orientational and angular momentum dependence is not additively separable. Put another way, the magnus moment does not come from either the orientational expansion (11) or the slow spin expansion (25) since each term contains factors from both. The lowest order Magnus moment is

$$K^i = c^i_{jk}\xi^j\omega^k \tag{27}$$

where the symbol c is re-used. Since the Magnus moment is only important for spinning projectiles, assume $\omega^1 \gg \omega^2$ and $\omega^1 \gg \omega^3$. Then,

$$\frac{K^2}{K^0} = C^2_{Mp}\omega^1\alpha\cos\varphi \tag{28a}$$

$$\frac{K^3}{K^0} = C^3_{Mp}\omega^1\alpha\sin\varphi \tag{28b}$$

This effect is not expected to be important for a railgun projectile, but is included in the NRL exterior ballistics model so that spinning projectiles can be treated.

IV. CFD SIMULATIONS AND BALLISTIC TRAJECTORIES

A. CFD Modeling of a Standard Bullet

In order to determine the ballistic coefficients discussed above, either experiments have to be devised and carried out, or an extensive CFD modeling effort has to be undertaken. Since the accuracy of the CFD models depends on the numerical mesh in a non-trivial way, it is important to carry out some form of code validation for various mesh parameters. Although the necessary data is not yet available for the projectile of interest, one can validate the CFD models using an existing, well characterized projectile. Evidently, one such projectile is the 0.308" 168 grain Sierra International (SI) bullet [2].

Fig. 4 shows a simulation of the SI bullet in flight at Mach 2.5. The pressure contours are calculated using the commercial code CFD++, produced by Metacomp, Inc., which will be used for all the CFD calculations in this report. The numerical meshes used in this work
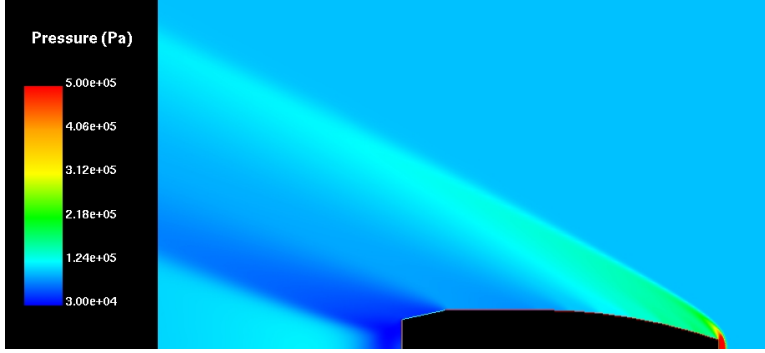
FIG. 4: False color image of pressure developed by the 168 grain Sierra International bullet at Mach 2.5, as computed by CFD++.

were created using Capstone Meshing and Geometry (MG) [3]. The double precision version of CFD++ is used throughout, because, for meshes with triangles as small as 100 μm, it was found that single precision calculations cannot reduce the residual below 10^{-4}. All the results reported here had residuals between 10^{-5} and 10^{-4}. CFD++ has a turbulence model [4], and supports a wall function technique for treating unresolved boundary layers. For the simulations reported here, the turbulence parameters were initialized with the values $k = 4.34$ m^2/s^2, and $\epsilon = 8610$ m^2/s^3. Here, k is the turbulent kinetic energy per unit mass, and ϵ is the energy dissipation rate per unit mass. The turbulent viscosity is $k^2/\epsilon = 0.0022$ m^2/s, similar to the viscosity of ambient air. The boundary conditions at the surface of the bullet were either inviscid surface tangency, or used a no-slip condition with a wall function. Capstone MG has the capability of creating boundary layer meshes, but these are not used in the present study.

Consider first numerical evaluation of the drag coefficient of the SI bullet, with various Mach numbers, mesh parameters, and boundary layer models. The drag coefficient is supposed to be insensitive to temperature and pressure, but for definiteness we consider an atmosphere with $T = 288$ K and $P = 1.01 \times 10^5$ Pa. For the zero-yaw drag, one may exploit axisymmetry, resulting in an effective two dimensional mesh. The six sets of mesh parameters used in this report are summarized in table I [8]. For the two dimensional cases, the mesh elements are triangular. The overall size of the mesh is characterized by the number of triangles. Generally the triangles are close enough to equilateral so that a single length, L, characterizes their size. The size of the smallest triangle in the mesh is $L_{\min}$ and the size of the largest one is $L_{\max}$. Note that although mesh B has smaller triangles than mesh C,

TABLE I: Parameters for Meshes

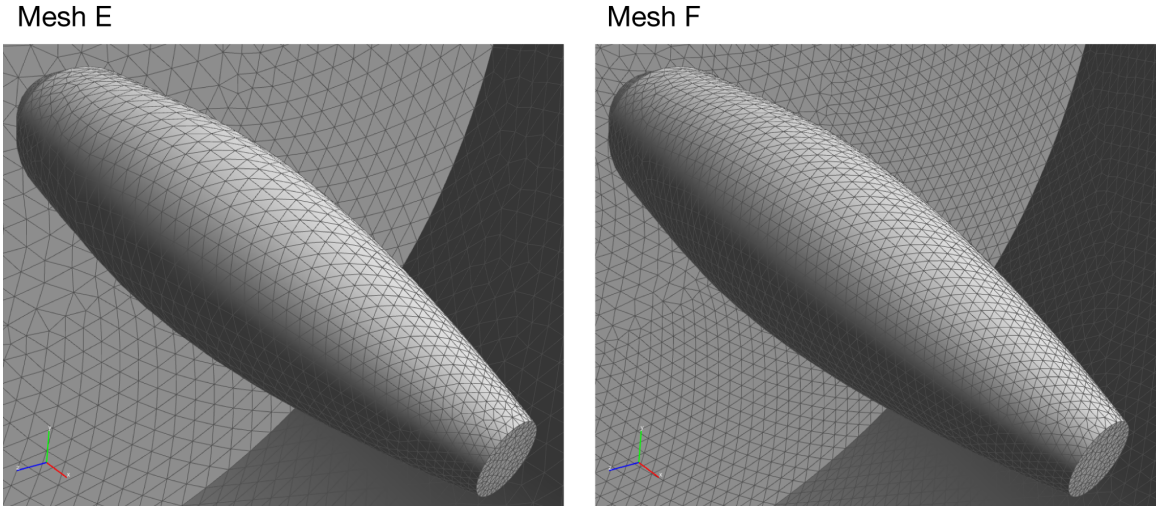| Mesh Label	Dimensions	Triangles or Tetrahedrons	$L_{\min}$ (calibers)	$L_{\max}$ (calibers)
A	2	486	0.14	6.0
B	2	7976	0.042	0.87
C	2	44895	0.053	0.49
D	2	134530	0.011	0.40
E	3	689431	0.019	2.29
F	3	2557714	0.019	1.45

Mesh E   Mesh F

FIG. 5: View of the two 3D meshes used in this report. Only the surface mesh is shown.

mesh C has many more triangles. This is because for mesh B, the triangles are allowed to grow more rapidly as the distance from the body is increased. The practice of growing the triangles in this way follows from the expectation that the highest resolution is needed near the body.

The effect of the boundary layer model is illustrated in Fig. 6, where the drag coefficients given in [2] are compared with CFD++ calculations using $M = \{1.4, 1.8, 2.0, 2.2, 2.5\}$ and mesh D. The results of using inviscid surface tangency are shown in Fig. 6(a), while the results of using the wall function technique are shown in Fig. 6(b). The inviscid surface tangency condition gives results that are accurate to three digits for $M = 1.4$, 1.8, and 2.5. For $M = 2.0$ and 2.2, the error is similar for either boundary condition. The fact
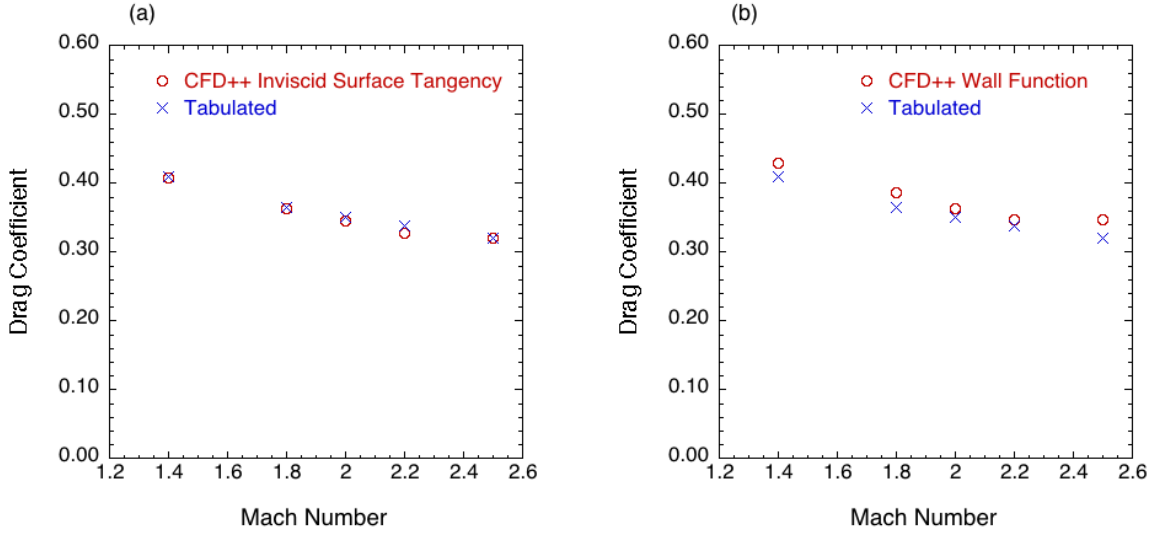
FIG. 6: Comparison of drag coefficients as computed by CFD++ with tabulated values from [2]. In (a), the calculation uses an inviscid surface tangency condition for the bullet. In (b), the calculation uses a wall function to approximate the effects of the boundary layer. The wall function tends to over-estimate the viscous drag, which for the considered parameters appears to be negligible.

that the wall function over-estimates the drag in every case, while inviscid surface tangency produces accurate results in most cases, suggests that the viscous drag, for the parameters considered, is in reality negligible. In the examples considered, the Reynolds number, Re, ranges between 10^5 and 10^6. The boundary layer thickness is $\sim \ell/\sqrt{Re} \approx 10$ μm, so that the total mass of the fluid in regions of shear flow is very small. Therefore, the momentum transferred from the body to the shear flow region is also small, and for the purpose of computing the drag coefficient, one might as well neglect the boundary layer altogether.

The effect of the various mesh parameters on the accuracy of the computed drag coefficient is illustrated in Fig. 7. The accuracy of a given mesh is characterized by the root-mean-squared (RMS) deviation from the known data:

$$\langle \delta C_D^2 \rangle^{1/2} = \sqrt{\frac{1}{N} \sum_{i=1}^{N} [C_D(M_i) - C_D^*(M_i)]^2} \tag{29}$$

Here, M_i is the set of Mach numbers considered, C_D is the drag coefficient as computed using a particular mesh, and C_D^* is the tabulated drag coefficient from [2]. The RMS error
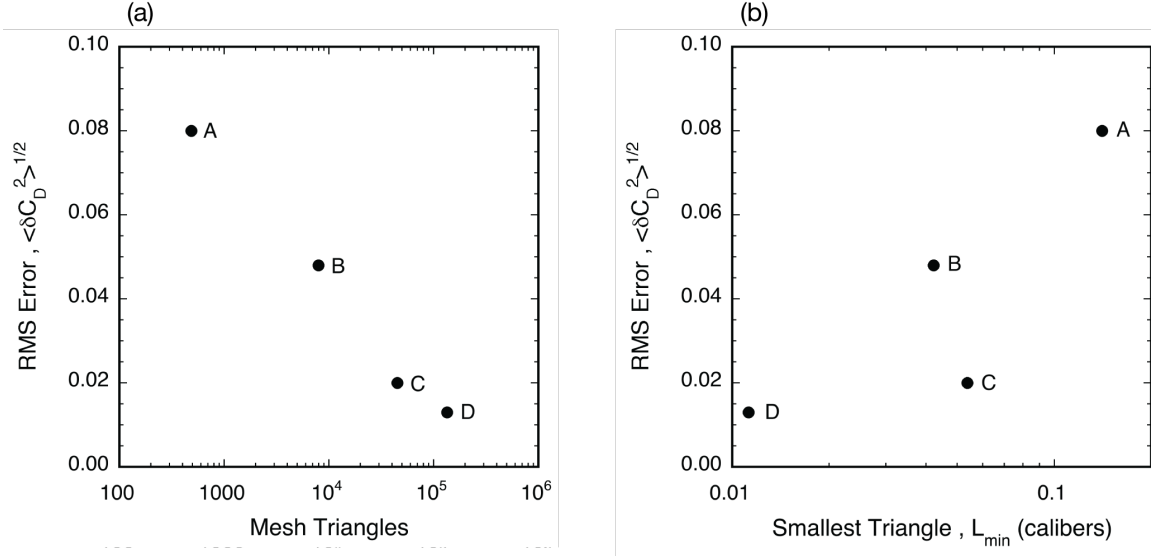
FIG. 7: Effect of mesh parameters on accuracy of drag coefficient: (a) RMS error in drag coefficient as a function of the total number of triangles in the mesh, and (b) as a function of the size of the smallest triangle. The progression in (b) is not monotonic due to the effect of the different growth rate of the triangles used in meshes B and C.

vs. the number of mesh triangles is shown in Fig. 7(a). As expected, the error diminishes with increasing number of triangles, although not very rapidly. When plotted vs. $L_{\min}$, the error does not vary monotonically. In particular, the error for mesh C is smaller than that for mesh B, even though mesh B has a slightly smaller $L_{\min}$. Evidently, the larger number of triangles associated with mesh C, which corresponds to a smaller ∇L, improves the accuracy of the calculation substantially. Similarly, comparing the accuracy of C and D shows that decreasing $L_{\min}$ a factor of five, while holding $L_{\max}$ roughly fixed, reduces the error by less than a factor of two. The conclusion is that both $L_{\min}$ and ∇L should be small, which generally means $L_{\max}$ should be small and the number of triangles should be large.

In order to compute ballistic coefficients at non-zero yaw angles, three dimensional simulations are required. The coefficients for a given Mach number are recovered by fitting the quasi-expansion to the simulated forces and moments at several yaw angles. One simulation is needed for each yaw angle. This process has to be repeated for each Mach number. In this report seven yaw angles at a single Mach number of $M = 2.5$ are considered. The simulation results are summarized in Fig. 8. The simulations agree rather roughly with the tabulated data, for both meshes E and F. In the case of the drag data of Fig. 8(b), it is
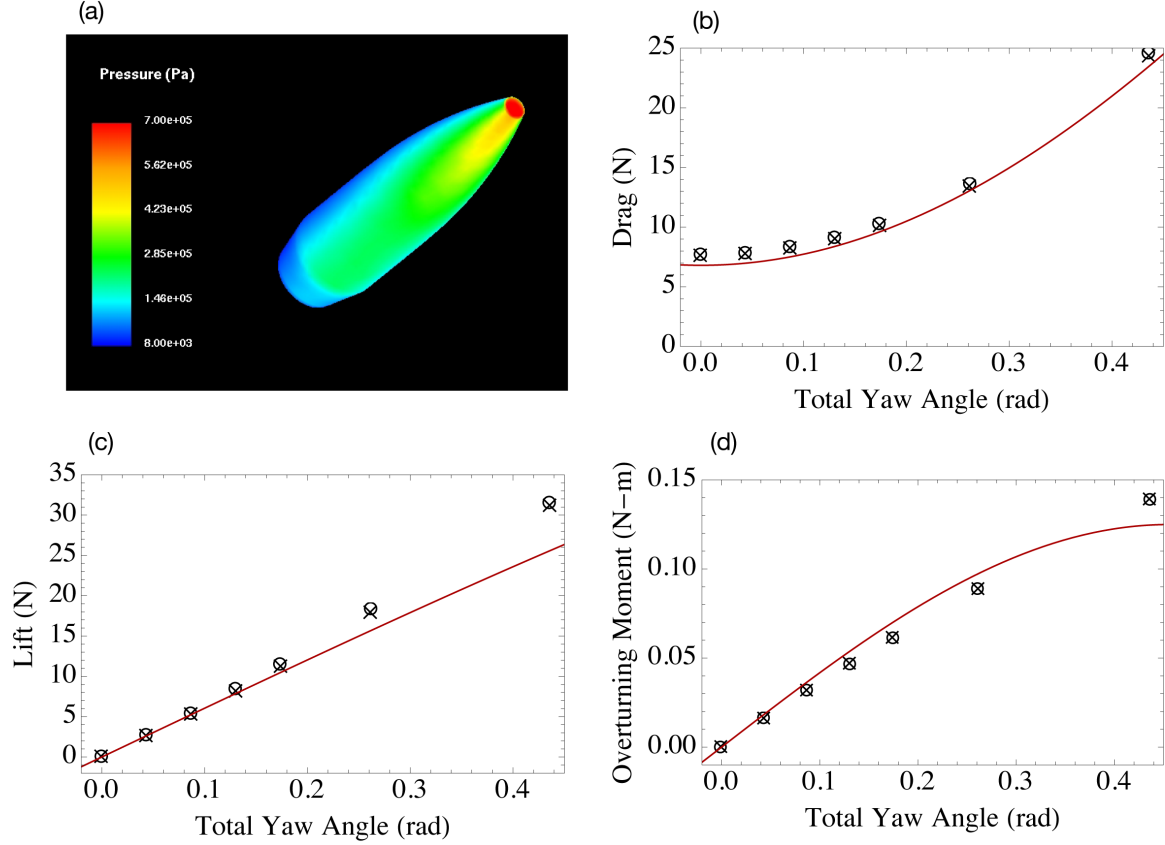
FIG. 8: CFD++ simulations in three dimensions of the SI bullet at Mach 2.5: (a) pressure on the surface of the bullet for $\alpha = 0.44$, (b) drag force vs. α, (c) lift force vs. α, and (d) overturning moment vs. α. The open circles are the results using mesh E, the crosses are the results using mesh F, and the curves are drawn using ballistic coefficients from [2]. The ballistic coefficients implied by the simulation data can be determined by fitting the data to the quasi-expansion in $\sin \alpha$, leading to the results given in table II.

not surprising that the simulation over-estimates the drag force, since the same trend is exhibited by axisymmetric simulations. In three dimensions it is even more difficult to use enough cells to obtain high accuracy. In the case of the lift data of Fig. 8(c), the simulation data is quite accurate for small angles. Since Ref. [2] does not provide data on the cubic lift coefficient, the divergence of the results at large angles is not a concern. In the case of the overturning moment data of Fig. 8(d), the primary source of disagreement is that the simulation underestimates the cubic term.

Using the data from mesh F, the angular dependence of the drag force, lift force, and overturning moment, are fitted to the quasi-expansion to obtain the ballistic coefficients.

TABLE II: Ballistic Coefficients Computed on Mesh F

Coefficient	CFD++	Tabulated
C_{D0}	0.349	0.320
$C_{D\alpha^2}$	4.4	4.4
$C_{L\alpha^0}$	2.97	2.85
$C_{L\alpha^2}$	2.84	n/a
$C_{M\alpha^0}$	2.15	2.56
$C_{M\alpha^2}$	-0.96	-4.4

These are displayed in table II alongside the data from Ref. [2]. The largest disagreement occurs for the cubic overturning moment.

B.   Ballistics Modeling of a Standard Rifle Shot

In order to verify that the generalized ballistics model developed in this report reduces to the correct solution for a standard rifle shot, trajectories are computed for the 168 grain SI bullet. The parameters for the shot are taken from Ref. [2]. The atmospheric conditions are $T = 288.15$ K and $\rho = 1.225$ kg/m^3. The conditions at the muzzle are $v = 792$ m/s, $\mathbf{\Omega} \cdot \mathbf{v}_1 = 16336$ rad/s, $\mathbf{\Omega} \cdot \mathbf{v}_2 = 25$ rad/s, $\mathbf{\Omega} \cdot \mathbf{v}_3 = 0$, and $\mathbf{v}_1 \cdot \mathbf{e}_2 = \sin(50.46')$ (the shot is elevated by 50.46 minutes of arc, which is supposed to result in grounding at 1000 yards). Initially, $\mathbf{b}_i \cdot \mathbf{v}_i = 1$, for each i. The rotation of the Earth is neglected. The reduction to a rigid, axisymmetric body is accomplished by taking $\mathbf{a} = 0$, $\delta\mathsf{M} = 0$, and by applying the transformations in table IV.

The epicyclic pitch and yaw phenomenon associated with spinning projectiles leads to orbits in phase space that offer obvious visual cues when two calculations give different results. In particular, it is useful to display parametric plots of the pitch and yaw angles, with time as the parameter. Here, the pitch angle is defined as $\sin^{-1}(\mathbf{v}_2 \cdot \mathbf{b}_1)$ and the yaw angle is defined as $\sin^{-1}(\mathbf{v}_3 \cdot \mathbf{b}_1)$. The parametric plots are displayed in Figs. 9 (a), (b), and (c). The full solution is shown in (a), which should be, and is, indistinguishable from Fig. 9.2 of Ref. [2]. The solution in (b) is the result when the magnus moment is neglected. Although the magnus effect is small, the effect of neglecting it is discernable. The solution
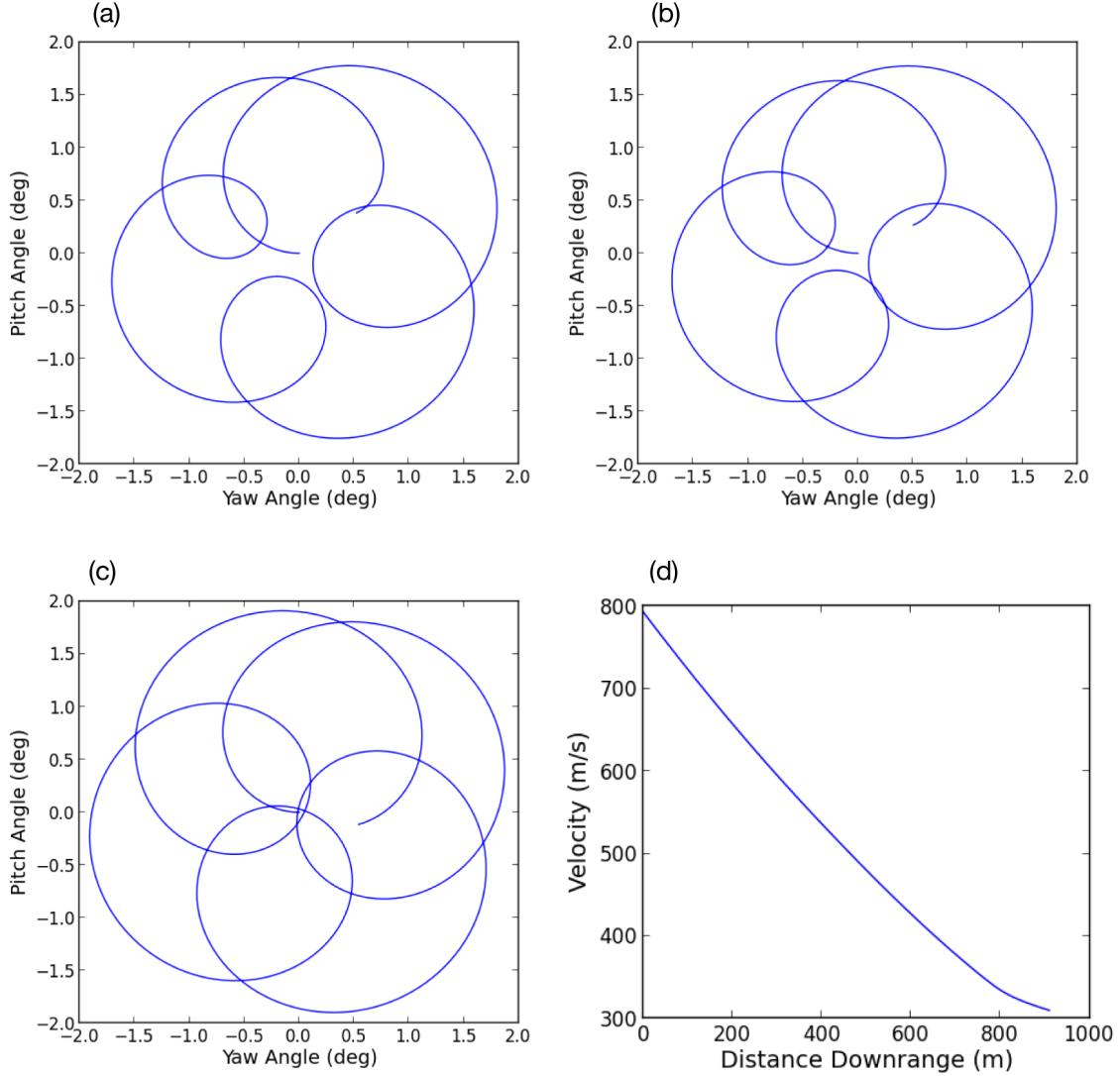
FIG. 9: Calculation of a standard rifle shot trajectory using NRL ballistics code. The epicyclic pitch and yaw during the first 15 yards is shown for (a) the full set of forces and moments, (b) without magnus moment, and (c) without pitch damping moment. The velocity as a function of range is given in panel (d).

in (c) is the result when the pitch damping moment is neglected. The velocity of the bullet over several hundred meters, with all forces and moments included, is shown in Fig. 9(d). The knee in the curve around 800 meters is due to passage through the transonic regime.

The vertical and horizontal position of the bullet is shown in Fig. 10. The upper panel shows the height of the bullet above the ground vs. range. The bullet is grounded after 1000 yards (914 meters), exactly as expected. The lower panel shows the horizontal drift of
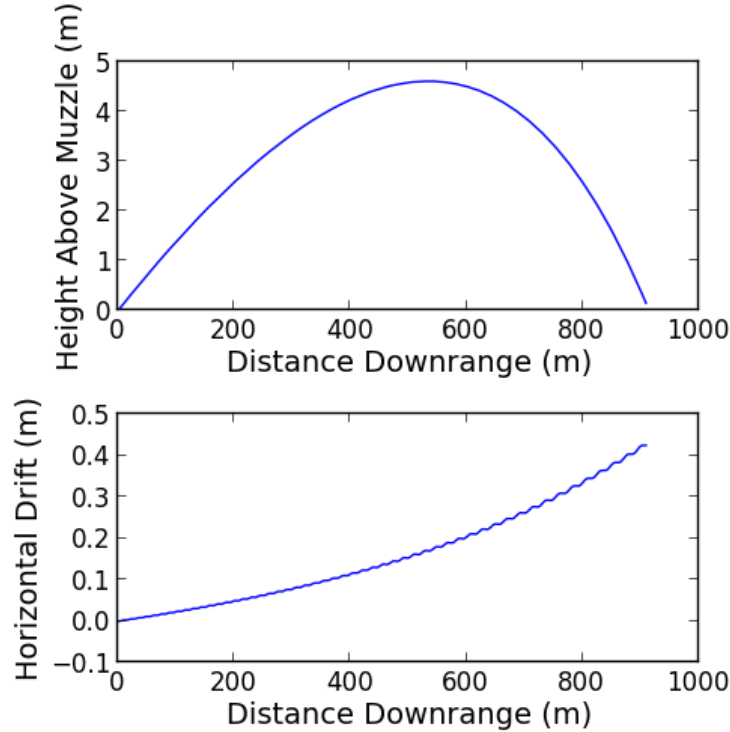
FIG. 10: Calculation of a standard rifle shot trajectory using NRL ballistics code, showing vertical position, $\mathbf{R} \cdot \mathbf{e}_2$ and horizontal position, $\mathbf{R} \cdot \mathbf{e}_3$, of the 168 grain Sierra International bullet.

the bullet over the same range. The drift in the positive $\mathbf{e}_3$ direction comes about because of the positive sign of $\mathbf{\Omega} \cdot \mathbf{e}_2$ at the muzzle. The periodic swerving motion of the bullet can be seen, particularly near the end of its range.

C. Preliminary Smart Bullet Modeling

A smart bullet is a bullet with a steering mechanism and an autopilot. The theory and practice of autopilots is, of course, highly developed [5]. In this section an extremely simple autopilot is used to demonstrate the viability of skid weight steering. This simple autopilot is capable of correcting up to 5 degree aiming errors at 150 meters.

Autopilots are often categorized as skid to turn (STT) or bank to turn (BTT). The abstract projectile design in Fig. 2 allows for either. If the skid weight is allowed to move in a plane, it provides an STT capability. The roll wheel allows for BTT capability, when complemented by linear motion of the skid weight. In this preliminary test, only the STT capability is employed. The ballistic coefficients correspond to a stabilized 168 grain SI

bullet. The stabilization (using fins, say) is assumed to lead to $C_{M\alpha^0} = -0.1$, and $C_{L\alpha^0} = 3.0$, at all times during the flight. The numerical shot is taken from a barrel without any rifling (the projectile does not spin). The mass of the skid weight is $\delta m/m = 0.02$. Roughly, the autopilot moves the skid weight in the direction of the target, and opposite the direction of the velocity. Specifically,

$$\delta\mathbf{v} \cdot \mathbf{b}_1 = 0 \tag{30a}$$

$$\delta\mathbf{v} \cdot \mathbf{b}_2 = \delta v_0 \tanh\left[\mathcal{A}(\mathbf{t}_1 - \mathbf{v}_1) \cdot \mathbf{b}_2\right] \tag{30b}$$

$$\delta\mathbf{v} \cdot \mathbf{b}_3 = \delta v_0 \tanh\left[\mathcal{A}(\mathbf{t}_1 - \mathbf{v}_1) \cdot \mathbf{b}_3\right] \tag{30c}$$

where δv_0 is the maximum velocity of the skid weight, $\mathcal{A}$ is a dimensionless parameter characterizing how sensitive the velocity is to misalignments, and $\mathbf{t}_1$ is a unit vector in the direction of the target. In the following example, $\delta v_0 = 0.03$ m/s, and $\mathcal{A} = 10$. The displacement of the skid weight is limited to 3 millimeters.

The results from the calculation are shown in Fig. 11. The shot is deliberately aimed to the right of the target by 4° (when looking downrange). The vertical aim is dead-on, but does not account for gravity. The target is 150 meters from the muzzle. Figs. 11(a) and (b) show that when the autopilot is off, the bullet misses the target by 10 meters. Figs. 11(c) and (d) show that with the autopilot, the bullet hits the target to within a few centimeters.

V. CONCLUSIONS

Full trajectory modeling of non-axisymmetric, hypervelocity projectiles can be modeled using the ballistics code described in this report. The form of the forces and moments, for small angles of attack, can be deduced from symmetry principles. The model includes a provision for internal moving parts that allow for steering of the projectile. A simple autopilot example shows that steering by means of an internal skid weight is viable, in principle. In order to apply the ballistics model to a real railgun projectile, which may have a novel shape, extensive CFD calculations have to be carried out. The commercial code CFD++ reproduces published drag coefficients on a well resolved axisymmetric mesh. Three dimensional calculations are more challenging due to the need for very large numbers of tetrahedrons, but preliminary simulations reproduce the most important ballistic coefficients, to within about 10%, for small angles of attack. The CFD results might be improved by using a
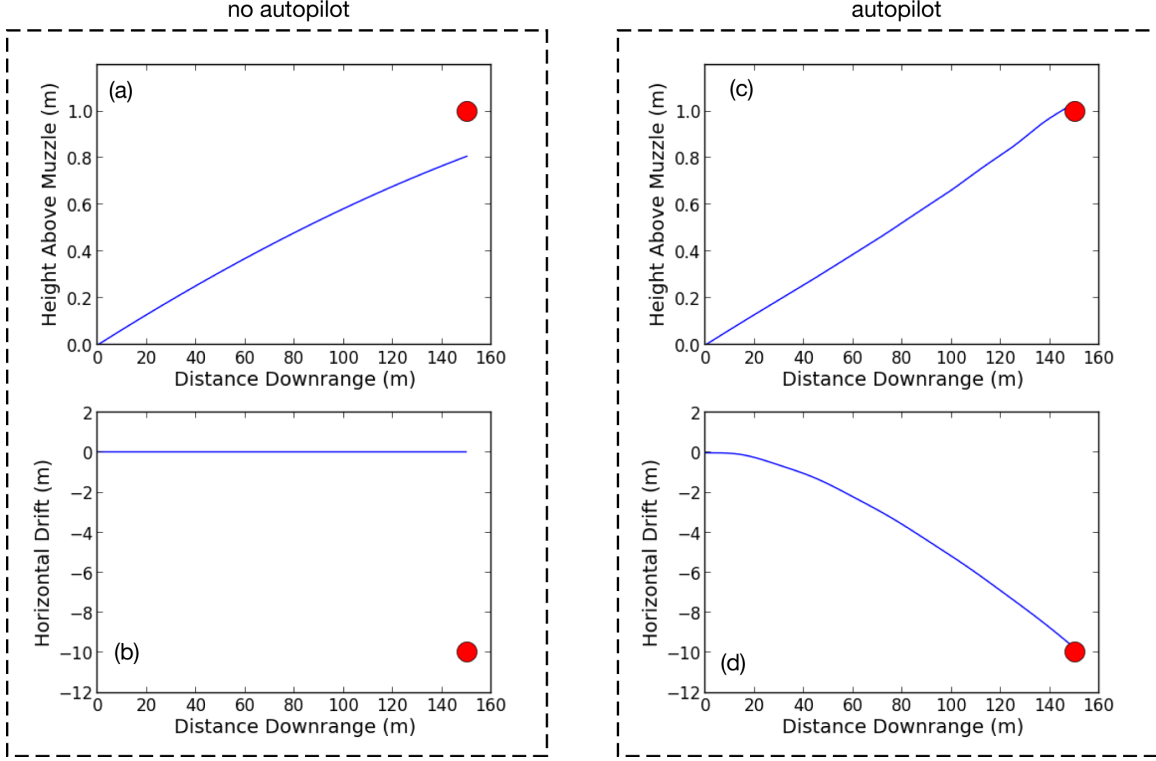
FIG. 11: Trajectory of 168 grain SI bullet with and without a simple STT autopilot: (a) vertical plane without autopilot, (b) horizontal plane without autopilot, (c) vertical plane with autopilot, and (d) horizontal plane with autopilot. The target is shown as the red circle.

boundary layer mesh, or increasing the number of tetrahedrons.

VI. ACKNOWLEDGEMENTS

[1] L.D. Landau and E.M. Lifschitz. *Fluid Mechanics.* Pergamon Press, Oxford, England, 1980.

[2] R.L. McCoy. *Modern Exterior Ballistics.* Schiffer, Atglen PA, 2012.

[3] R. Aubry, B.K. Karamete, E.L. Mestreau, and S. Dey. A three-dimensional parametric mesher with surface boundary-layer capability. *J. Comp. Phys. (accepted)*, 2014.

[4] U. Goldberg, O. Peroomian, P. Batten, and S. Chakravarthy. The $k-\epsilon-R_t$ turbulence closure. *Engineering Applications of Computational Fluid Mechanics*, 3(2):175–183, 2009.

[5] Bernard Etkin and Lloyd Duff Reid. *Dynamics of flight: stability and control.* Wiley, 3 edition, Oct 1995.

[6] This should not be confused with a specification of which coordinate system the components of $\delta\mathbf{v}$ are expressed in. By definition, vector equations are valid in any basis.

[7] We distinguish covariant and contravariant indices for the sake of the summation convention. In Euclidean geometry, the metric tensor is the identity, and the components of a covariant, mixed, or contravariant tensor are the same.

[8] Ballisticians often measure lengths in calibers, where 1 caliber is the diameter of the bullet under study. Perhaps confusingly, the phrase "0.308 caliber bullet" refers to (i) a bullet with diameter 0.308 inches, and (ii) a unit of length of 0.308 inches, called a caliber.

Appendix A: Transformation from Velocity Basis to Body Basis

The ballistic coefficients utilized in this report are given in terms of the body system of coordinates. That is, the forces and moments are resolved in directions parallel and perpendicular to the axes of inversion symmetry. Many tables of ballistic coefficients for axisymmetric projectiles are given in the velocity system of coordinates. That is, the forces and moments are resolved in directions parallel and perpendicular to the effective velocity.

In order to connect the ballistic coefficients in the two commonly used coordinate systems, it is most convenient to express the total forces and moments in terms of abstract vector formulas. This is done in table III. If the components are expressed in the body basis, and the resulting expressions expanded in powers of $\sin\alpha$ (the quasi-expansion should be used in this context, including multiplication of the axial force by $\cos\alpha$), it is straightforward to

TABLE III: Vector Forces and Moments for Axisymmetric Projectiles

Name	Formula
Drag Force	$-F^0(C_{D0} + C_{D\alpha^2}\alpha^2)\mathbf{v}_1$
Lift Force	$F^0(C_{L\alpha^0} + C_{L\alpha^2}\alpha^2)\mathbf{v}_1 \times (\mathbf{b}_1 \times \mathbf{v}_1)$
Overturning Moment	$K^0(C_{M\alpha^0} + C_{M\alpha^2}\alpha^2)\mathbf{v}_1 \times \mathbf{b}_1$
Spin Damping Moment	$K^0 C_{lp}\mathbf{b}_1(\omega \cdot \mathbf{b}_1)$
Pitch Damping Moment	$K^0 C_{Mq}\mathbf{b}_1 \times (\omega \times \mathbf{b}_1)$
Magnus Moment	$K^0 C_{Mp}(\omega \cdot \mathbf{b}_1)\mathbf{b}_1 \times (\mathbf{v}_1 \times \mathbf{b}_1)$

TABLE IV: Transformation of Ballistic Coefficients for Axisymmetric Projectiles

Effect	Body Coefficients	Velocity Coefficients
Zero Yaw Axial Force	$C_{X\alpha^0}$	$-C_{D0}$
Yaw Axial Force	$C_{X\alpha^2 c} = C_{X\alpha^2 s}$	$-C_{D\alpha^2} + C_{L\alpha^0}$
Linear Normal Force	$C_{N\alpha^0}^i$	$-C_{D0} - C_{L\alpha^0}$
Cubic Normal Force	$C_{N\alpha^2 c}^i = C_{N\alpha^2 s}^i$	$\frac{1}{2}C_{L\alpha^0} - C_{D\alpha^2} - C_{L\alpha^2}$
Roll Righting Moment	C_{Mr}	0
Linear Overturning Moment	$C_{M\alpha^0}^2$	$C_{M\alpha^0}$
Cubic Overturning Moment	$C_{M\alpha^2 c}^2 = C_{M\alpha^2 s}^2$	$C_{M\alpha^2}$
Linear Overturning Moment	$C_{M\alpha^0}^3$	$-C_{M\alpha^0}$
Cubic Overturning Moment	$C_{M\alpha^2 c}^3 = C_{M\alpha^2 s}^3$	$-C_{M\alpha^2}$
Spin Damping Moment	C_{Mq}^1	C_{lp}
Pitch Damping Moment	C_{Mq}^i	C_{Mq}
Magnus Moment	C_{Mp}^i	C_{Mp}

collect like powers, thereby determining the body coefficients. The result of this procedure is summarized in table IV. In the table, the superscript i refers to either the $\mathbf{b}_2$ or $\mathbf{b}_3$ direction.

Appendix B: Ballistic Coefficients in Terms of Tensor Coefficients

The ballistic coefficients derived in this report are related to the coefficients in a more general tensor expansion. The tensor coefficients are denoted by a, b, c, etc.. There are

four sets of such tensor coefficients, one for the forces, one for the orientation-dependent moments, one for the spin-dependent moments, and one for the Magnus moment. In order to avoid notational clutter, the same alphabetic sequence is used in each of the four cases, despite the fact that each tensor expansion is independent.

Each ballistic coefficient is proportional to a sum of tensor coefficients. Table V lists all the ballistic coefficients considered herein, and the particular combination of tensor coefficients that each is proportional to. The constant of proportionality contains factors such as F^0 for a force, K^0 for a moment, and possibly expressions involving orientational angles and normalized angular velocities.

The information in table V is not needed to carry out an exterior ballistics calculation, nor to determine the ballistic coefficients, which have to be determined from CFD calculations or experiments. It is provided only for completeness.

TABLE V: Ballistic and Tensor Coefficients

Coefficient	Symbol	Tensor Expansion
Axial Force	$C_{X\alpha^0}$	$a^1 + b_1^1 + c_{11}^1 + d_{111}^1$
Axial Force	$C_{X\alpha^2 c}$	$-\frac{1}{2}b_1^1 - c_{11}^1 + c_{22}^1 - \frac{3}{2}d_{111}^1 + 3d_{122}^1$
Axial Force	$C_{X\alpha^2 s}$	$-\frac{1}{2}b_1^1 - c_{11}^1 + c_{33}^1 - \frac{3}{2}d_{111}^1 + 3d_{133}^1$
Normal Force	$C_{N\alpha^0}^2$	$b_2^2 + 2c_{12}^2 + 3d_{112}^2$
Normal Force	$C_{N\alpha^2 c}^2$	$-c_{12}^2 - 3d_{112}^2 + d_{222}^2$
Normal Force	$C_{N\alpha^2 s}^2$	$-c_{12}^2 - 3d_{112}^2 + 3d_{332}^2$
Normal Force	$C_{N\alpha^0}^3$	$b_3^3 + 2c_{13}^3 + 3d_{113}^3$
Normal Force	$C_{N\alpha^2 c}^3$	$-c_{13}^3 - 3d_{113}^3 + d_{333}^3$
Normal Force	$C_{N\alpha^2 s}^3$	$-c_{13}^3 - 3d_{113}^3 + 3d_{223}^3$
Roll Righting Moment	C_{Mr}	$c_{23}^1 + 3d_{123}^1$
Overturning Moment	$C_{M\alpha^0}^2$	$b_3^2 + 2c_{13}^2 + 3d_{113}^2$
Overturning Moment	$C_{M\alpha^2 c}^2$	$-c_{13}^2 - 3d_{113}^2 + 3d_{223}^2$
Overturning Moment	$C_{M\alpha^2 s}^2$	$-c_{13}^2 - 3d_{113}^2 + d_{333}^2$
Overturning Moment	$C_{M\alpha^0}^3$	$b_2^3 + 2c_{12}^3 + 3d_{112}^3$
Overturning Moment	$C_{M\alpha^2 c}^3$	$-c_{12}^3 - 3d_{112}^3 + 3d_{332}^3$
Overturning Moment	$C_{M\alpha^2 s}^3$	$-c_{12}^3 - 3d_{112}^3 + d_{222}^3$
Spin Damping Moment	C_{Mq}^1	b_1^1
Pitch Damping Moment	C_{Mq}^2	b_2^2
Pitch Damping Moment	C_{Mq}^3	b_3^3
Magnus Moment	C_{Mp}^2	c_{13}^2
Magnus Moment	C_{Mp}^3	c_{12}^3